P7.1 TURBULENCE IN MCS ANVILS: OBSERVATIONS AND ANALYSES FROM BAMEX

Randall Collander[2], Brian D. Jamison[2], Edward I. Tollerud[1], Fernando Caracena[1], Chungu Lu[2]
and Steven E. Koch[1]
[1]NOAA Research – Earth System Research Laboratory, Global Systems Division
Boulder, CO
[2]Cooperative Institute for Research in the Atmosphere (CIRA), Fort Collins, CO

1. INTRODUCTION

The occurrence of large mesoscale convective systems (MCSs) during the warm season over much of the central United States presents a hazard to aviation that has not been thoroughly assessed. In addition to lightning and hail, the extensive mid- to upper-level anvil clouds that form in these systems can cause severe turbulence. Although avoidance of the most intense convection in these areas by passenger aircraft and general aviation is usually possible, it is advantageous to know the risk of turbulence in regions within and close to the anvil clouds. If the risk can be determined, aircraft travel through these large anvils could become acceptable. Furthermore, if an algorithmic estimate of this risk could be developed, it could contribute to turbulence forecasting and warning.

Unfortunately, avoidance also means that observations within MCSs are few. During the Bow Echo and Mesoscale Convective Vortex Experiment (BAMEX; Davis *et al.*, 2002) held in the central United States in summer 2003, however, several mid-troposphere (2 to 4 km) research flights observed state and aircraft flight variables within and near the edges of large mesoscale anvils. A dropsonde aircraft (Learjet) flying at high levels was coordinated with two P-3 research aircraft below. During at least two of these flights (10 June and 23 June), the mission scientist and the lead cloud physics scientist on board the NOAA P-3 described in their logs several periods of moderate to heavy turbulence. These two and perhaps ten

Corresponding author address: Randall Collander, NOAA/ESRL, 325 Broadway R/GSD1, Boulder, CO 80305; e-mail randall.s.collander@noaa.gov.

other BAMEX missions offer the opportunity to diagnose turbulence episodes having dropsonde launches and in-situ aircraft measurements at mid-levels in anvil regions where the intensity and frequency of turbulence is relatively unknown.

We examine in detail the composite structure of the MCS that occurred on 10 June 2003 using observations from three project aircraft, Rapid Update Cycle (RUC) model data, and operational observation platforms. These observational and exploratory results lay the foundation for analyses of fields in regions where the possibility of air traffic exists and where there is high likelihood of turbulence as indicated by quantitative algorithms. Our analyses focus on near-anvil regions and on physical mechanisms (primarily mid-level rear inflow jets) that pose a turbulence threat. Based on these analyses, we discuss possible developments of more automated and quantitative assessment of the turbulence threat to general aviation and passenger airlines in the vicinity of anvil regions during mature and late stages of MCSs. Finally, we present observations from eight other BAMEX cases that are incorporated into a generalized composite profile of turbulence-sensitive parameters in the rear inflow region of MCSs.

2. DESCRIPTION OF THE BAMEX 10 JUNE MISSION

The BAMEX aircraft missions on 10 June (IOP7A) observed a bow echo that initially developed in eastern Nebraska (Davis et al. 2004). Three aircraft (the NOAA and NRL P-3's and the dropsonde Learjet) sampled the system from its early stages around 0100 UTC until 1100 UTC, when the anvil of the MCS was several hours past its greatest extent, but still large. Radar at 0540 UTC (Fig. 1) revealed a bowed line of very intense echoes in extreme northwest

Missouri and southwest Iowa. As Fig. 2 (bottom panel) illustrates, aircraft at this time were carefully avoiding the airspace occupied by the MCS. By 0809 UTC, an extensive anvil had formed behind and northeast of the convective line (Fig. 3). Some intrepid aircraft were now traversing the upper regions of the anvil volume (Fig. 2, top panel). As will be discussed later, the paucity of PIREPs within MCS anvils adversely impacts their use to confirm turbulence encounters in this study as well as in any other study of near-MCS turbulence episodes.

Since scheduled aircraft avoid MCS regions, only a limited number of PIREP (pilot report) observations of turbulence for this case or for any such system are available to provide useful confirmation (it should also be noted that the nocturnal nature of large MCSs minimizes anvil encounters). On the 10 June research flights, good confirmation for turbulence is provided by aircraft observations (*e.g.*, the NOAA P-3 accelerometer data (not shown) and by onboard scientist logs (for the NOAA P-3 mission, provided by Dave Jorgenson and Brian Jewett). Both noted several periods of moderate to severe turbulence.

2.2 PHYSICAL MECHANISMS

Much of the turbulence experienced by research aircraft during IOP7A was undoubtedly of convective origin, particularly during the close approaches to the convective line (*cf.* Fig. 1). However, within the anvil at a distance from the leading convective line, other turbulence-generating mechanisms might also be present, including shear-generated turbulence above and below the rear inflow jet. The dropsonde observation at 0526 UTC (Fig. 6) shows a distinct signature of the jet close behind the leading convective edge, and may be a preferred location for the development of turbulence. In fact, the section through the rear inflow region displayed in Fig. 7 (based on a reasonably straight line of dropsonde observations approximately transverse to the inflow jet; cf. the dropsonde locations show in Fig.3 in Eastern Nebraska identified by times between 0413 and 0526 UTC) reveals a strong jet near 500 hPa. The

vertical section of Richardson Number Ri (a proxy for the existence of turbulence) in Fig. 8 shows small near-critical values for Ri at altitudes just below the jet core in a layer of strong vertical wind shear.

Also in Fig. 8, the regions of low Ri near 350 hPa and above 250 hPa in the early (left half) of the section result from a strong upper-level jet streak (Fig. 7), a feature also found in profiler observations (not shown) and which may be related to upper-level MCS outflow. A clear example of this mechanism is shown in the Slater, Iowa wind profiler time section in Fig. 9. For several hours starting about 0500 UTC, when the Slater profiler was within the northern margins of the anvil (Figs. 1 and 3) there is a marked turning and acceleration of the upper-tropospheric (anvil top) winds. Development of jet streaks such as these is commonly noted in the environment of large MCSs (Maddox 1983) and is likely the result of MCS-synoptic scale interaction. In these regions during mature to late stages of MCS development, there could be instances of shear-generated turbulence above or below these jet streaks and either within or to the north of the dissipating anvil cloud. Another example of the use of wind profiler data to detect strong outflow regions above MCS's and rear inflow jets is provided by Ralph et al. (1995). Analyses of this jet in the 10 June MCS and BAMEX cases has not been undertaken, and may prove elusive given that aircraft missions did not focus on this feature.

3. COMPOSITE STRUCTURE AND RUC ANALYSES

The capability to produce accurate 3-dimensional analyses that capture the important features of this MCS depends critically on the quality and density, as well as the fortuitous placement, of research and operational observations. To assess the feasibility of analyses, we have organized the scattered set of observations in two ways: by compositing them relative to the MCS, and by analyzing them via the RUC model assimilation system.

Locations of the set of atmospheric soundings (research dropsondes, wind profilers, mobile (MGLASS) surface-based

soundings, and special soundings from operational rawinsonde sites) available during the mission are shown in Fig. 10. A methodology to locate soundings relative to a satellite-derived mid-anvil reference point is demonstrated in Fig. 11. By identifying hourly "anchor points" (in this case, the subjectively-determined center of mass of the MCS anvil as displayed on water vapor imagery), observations can be located in a reference frame defined by the MCS anvil. The resulting distribution of observation points in quadrants radiating out from the anvil center is shown in Fig. 12 (profiler observations have not been included on the plot or in the subsequent analyses shown here). From this distribution, we have prepared preliminary within-quadrant composite profiles of wind and thermodynamic variables; resulting wind speed and Ri profiles from the NW quadrant are shown in Figs. 13 and 14. For comparison, we also show representative same-quadrant profiles from the RUC analysis at 0700 UTC. Although similar magnitudes and structure are seen (e.g., the layer of low Ri below ~2 km), the RUC low-level wind feature is not reflected on the composite. The nature of this difference and that of other features in the remaining quadrants remains to be determined with refined composite and/or analysis procedures. As the small population of close-in anvil-relative PIREPs (green circles in Fig. 12) suggests, commercial aircraft were skirting the MCS anvil. This necessarily limited their usefulness as possible confirmation of turbulence for interpreting the composite quadrant profiles.

Concerning the potential use of model analyses and forecasts to compute turbulence algorithms, the 0700 UTC 500 hPa RUC analysis (Fig. 15) shows evidence that it does have some grasp of the evolving MCS; note the evidence for strong rear inflow in roughly the correct position in extreme Southeastern Nebraska.

The RUC analyses of 700 hPa Ri at 0700 UTC (Fig. 16) indicates potential areas of low- to mid-level turbulence (low Ri values) in the region below the inflow jet, as well as beneath the anvil region in eastern Iowa. In Fig. 17, TKE values computed using DTF3 at 250 hPa show a gradient of increasing values eastward (downwind) of the anvil cloud shield, as well as north of the MCS in a region where new convection was forming. It is likely that these latter results reflect the influence of an upper level outflow jet (cf. Section 2.2).

During the BAMEX field phase, high-resolution 4km WRF model runs were performed in near-real time. Fig. 18 displays 6h forecasts for the 10 June MCS valid at 0600 UTC. Although the location of the squall line lags reality by 25-50 km (compare the reflectivity in Fig. 18b with Fig. 1), in most respects it is a quite good forecast. The rear inflow jet is clearly captured leading into the convective line at 850 hPa (Fig. 18a). We interpret the results from both this run and the larger-scale RUC simulation with cautious optimism for further detailed mesoscale modeling of this system. The forecast location of the rear inflow jet may be an indicator (qualitative or perhaps eventually quantitative) of the sort that could be incorporated as an element of a GTG anvil turbulence algorithm.

4. OTHER BAMEX CASES

Confidence in the generality of the features observed in the 10 June MCS would be strengthened if similar observed results could be found in other cases. Since it is generally assumed that the rear inflow jet is an essential mechanism of many, if not all, MCSs with squall-like near-surface features, we examined other BAMEX missions for evidence of such a jet. In all, eight other similar MCS cases with well-placed dropsonde observations were found in the BAMEX field project dataset. Skew-t thermodynamic diagrams produced from dropsondes dropped into the inflow regions of these systems are presented in Fig. 19. Because of size limitations, satellite pictures of each MCS could not be included in this abstract, but they are available at the URL http://bolas.fsl.noaa.gov/BAMEX/sat_rearjet. htm. Most of the cases exhibit a squall line feature propagating toward the east or southeast. The soundings for these cases were made between 50 and 100 km behind (typically west or northwest of) the leading convective lines. The MCS on 23 June was almost stationary when the sounding

observation was taken near the center of its anvil.

The wind and thermodynamic profiles from the nine cases are fairly similar. Although some (for instance, the 6 July case) have a more complicated vertical structure, in general, each has a deep moist adiabatic cloud layer (the MCS anvil) overlaying a region of dry adiabatic temperature lapse rate. The mid- to low-level wind maximum tends to be at the top of this latter layer, at pressures between 500 and 700 hPa, suggesting a descending jet. The wind maxima are all in the range of 50-60 kt, or about 25-30 m/s, and range in direction from southwesterly to northwesterly.

The consistency within this set of inflow profiles suggests the value of a "conceptual" picture that could form the basis for near-anvil turbulence indicators. What this picture might look like is shown in Fig. 20, which is a composite wind profile built from the set of nine MCS cases. Even in this composite visualization, there is a marked wind speed maximum of 22 m/s near 4 km above sea level (asl). It is reasonable to conclude that turbulence exists within the strong shear regions just above and below this jet, as suggested in the RUC analyses of turbulence algorithms at these levels in the 10 June case.

5. CONCLUSIONS AND FUTURE PLANS

The results shown suggest both the feasibility and the potential value of analyses of the kind described here toward the development of knowledge and schemes leading to improved forecasts of turbulence near and within upper and mid-tropospheric MCS anvils. Other turbulence mechanisms worthy of investigation include turbulence associated with gravity waves, as reported in Koch et al. (2005), and instability mechanisms near the anvil top and the freezing level. The wave intrinsic frequency and the sense of vertical energy propagation can both be determined using the "wave hodograph method" from individual dropsonde profiles. The retrieved wave source location can then be related to other mesoscale phenomena, such as the rear inflow jet.

From these maps and the analyses built up from observations, it might be possible to develop GTG algorithms to help to forecast turbulence in these situations. As the cursory examination of other mission days in Section 4 indicates, there are possible analysis methods applicable to development of these algorithms. Finally, although considerable work is still required, the model fields shown suggest the future possibility of quantitative forecasts for turbulence near MCS anvils.

6. ACKNOWLEDGMENTS

7. REFERENCES

Davis, C., *et al.*, 2004: The Bow-Echo and MCV EXperiment (BAMEX): Observations and opportunities. Bull. Amer. Meteor. Soc., **85**, 1075-1089.

Davis, C., et al., 2002: Science overview of the bow echo and MCV experiment. http://www.mmm.ucar.edu/bamex/science.html

Koch, S.E., B.D. Jamison, C. Lu, T.L. Smith, E.I. Tollerud, N. Wang, T.P. Lane, M.A. Shapiro, C.G. Girz, D.D. Parrish, and O.R. Cooper, 2005: Turbulence and gravity waves within an upper-level front. *J. Amos. Sci.* (in press)

Maddox, R. A., 1983: Large-scale meteorological conditions associated with midlatitude, mesoscale convective complexes. *Mon. Wea. Rev.*, **111**, 1475-1493.

Ralph, F.M., P. J. Neiman, D. W. Van de Kamp, and D. C. Law, 1995: Using spectral moment data from NOAA's 404-MHz radar wind profilers to observe precipitation. *Bull. Amer. Meteor. Soc.*, **76**, 1717–1739.
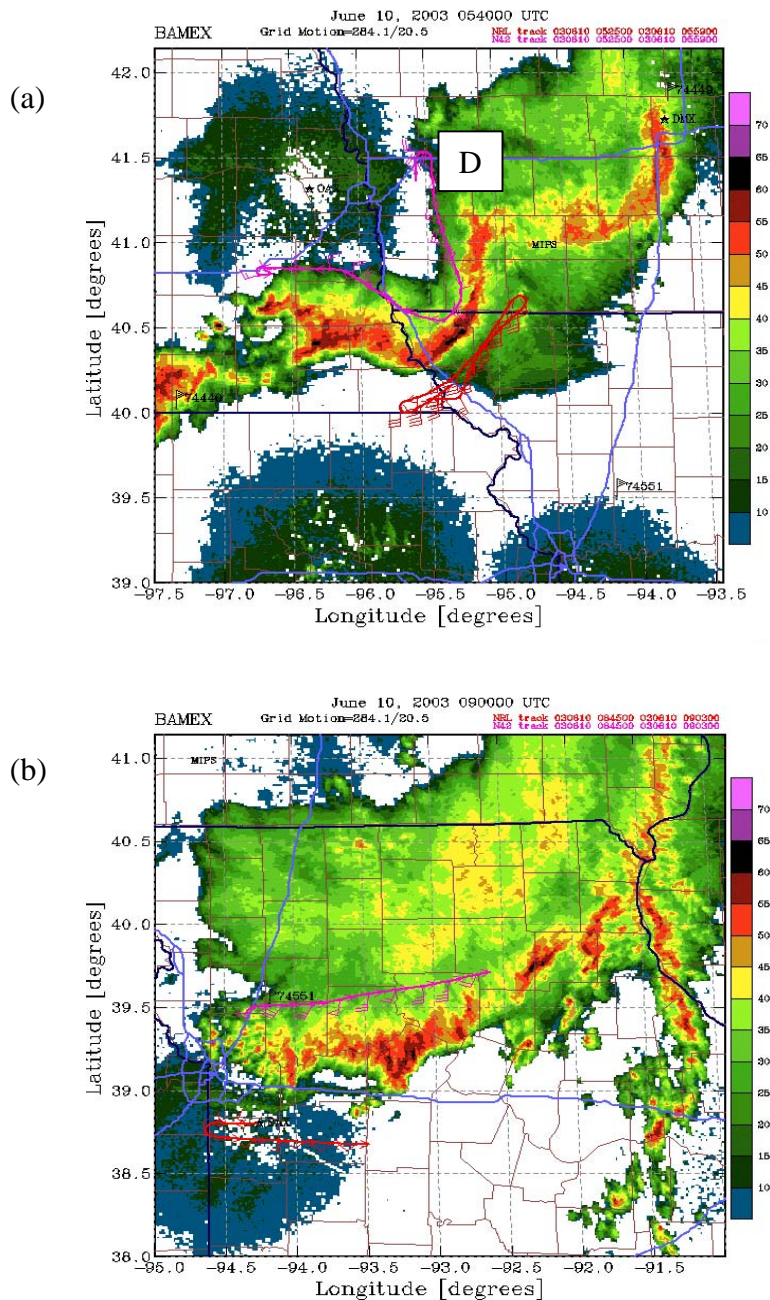
Fig. 1. NEXRAD radar observations at (a) 0540 UTC and (b) 0900 UTC on 10 June 2003. Simultaneous flight track segments for two P-3 aircraft are also shown; pink denotes the NOAA P-3 and red the NRL P-3. The location of the dropsonde launch at 0526 UTC is denoted as "D". Adapted from images available at http://www.ofps.ucar.edu/bamex/catalog/index.html
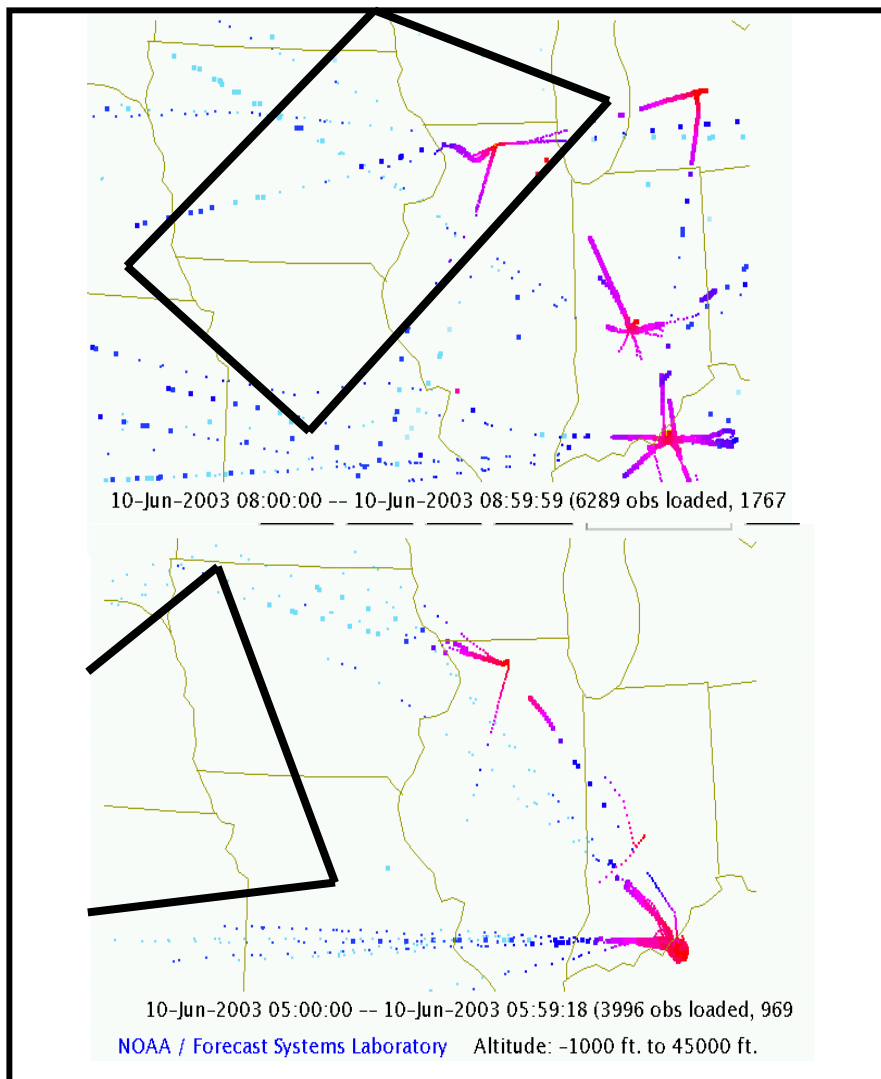
Fig. 2. Scheduled aircraft flight data reports (ACARS) for 1-h periods on 10 June 2003 starting at 0800 UTC (top panel) and 0500 UTC (bottom panel). Light and dark blue reports are at altitudes that would intersect the anvil clouds. See Figs. 3 and 1, respectively for location and extent of convective and anvil regions at these times; schematic cloud shields (denoted by heavy black lines) roughly delineate these areas. ACARS reports were accessed from the FSL ACARS website (http://acweb.fsl.noaa.gov/).
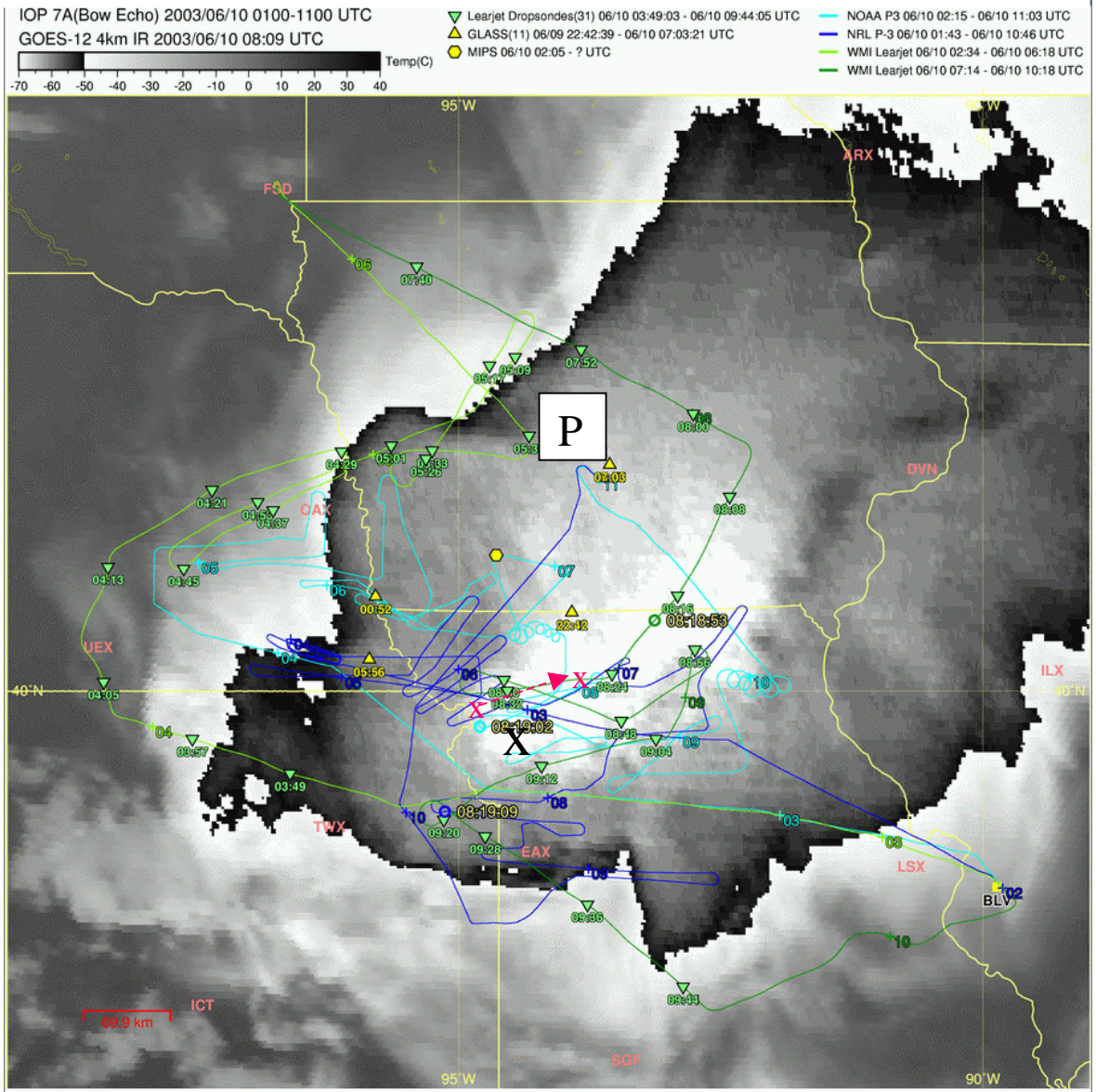
Fig. 3. Infrared satellite imagery at 0809 UTC 10 June 2003. The locations of aircraft tracks and dropsonde observations are superposed (note that tracks span the entire mission duration). "P" indicates the location of the Slater, Iowa, profiler (see text). Available from the UCAR JOSS BAMEX website at http://www.ofps.ucar.edu/bamex/catalog/index.html.
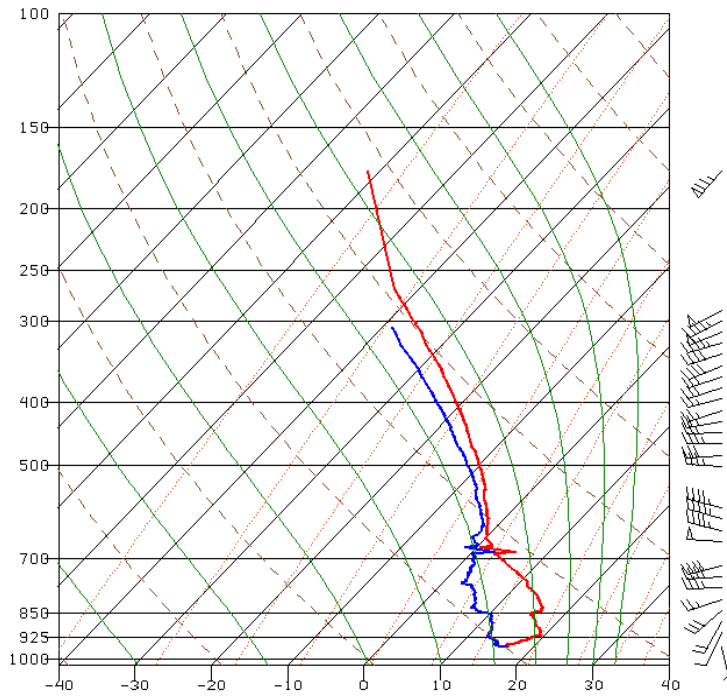
Fig. 6. Temperature and wind observations from Learjet dropsonde at 0526 UTC 10 June 2003. The location of this drop is shown on Fig. 1. From http://www.ofps.ucar.edu/bamex/catalog/index.html.
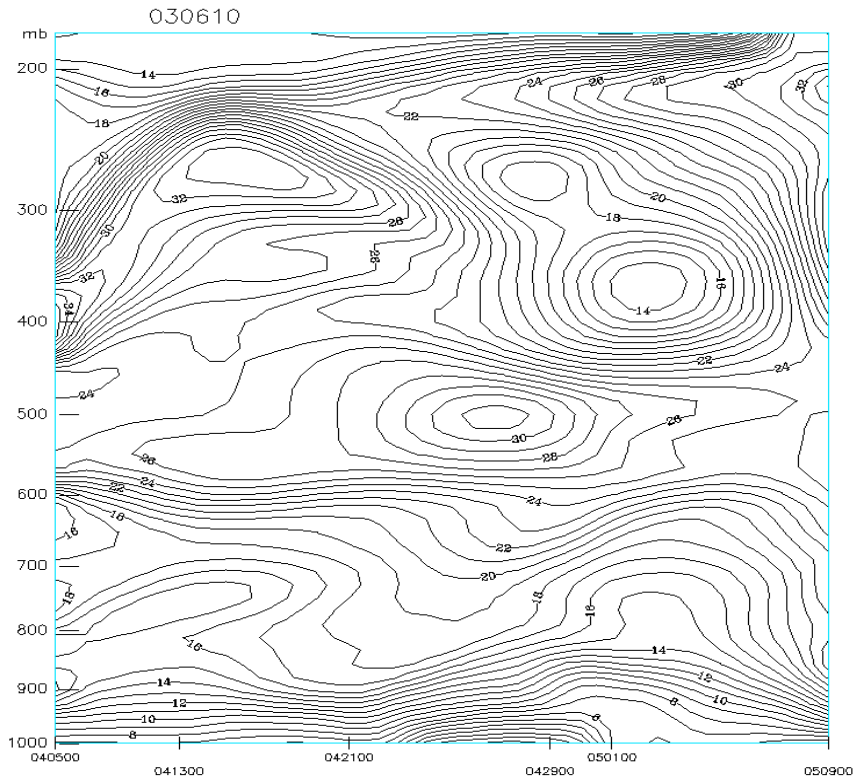
Fig. 7. Wind speed contours constructed from dropsonde observations in a section transverse to the rear inflow jet behind the squall line. Observation times indicated on the x axis can be collated on Fig. 3. To pinpoint section location relative to the MCS anvil, see the green triangles in East Central Nebraska.
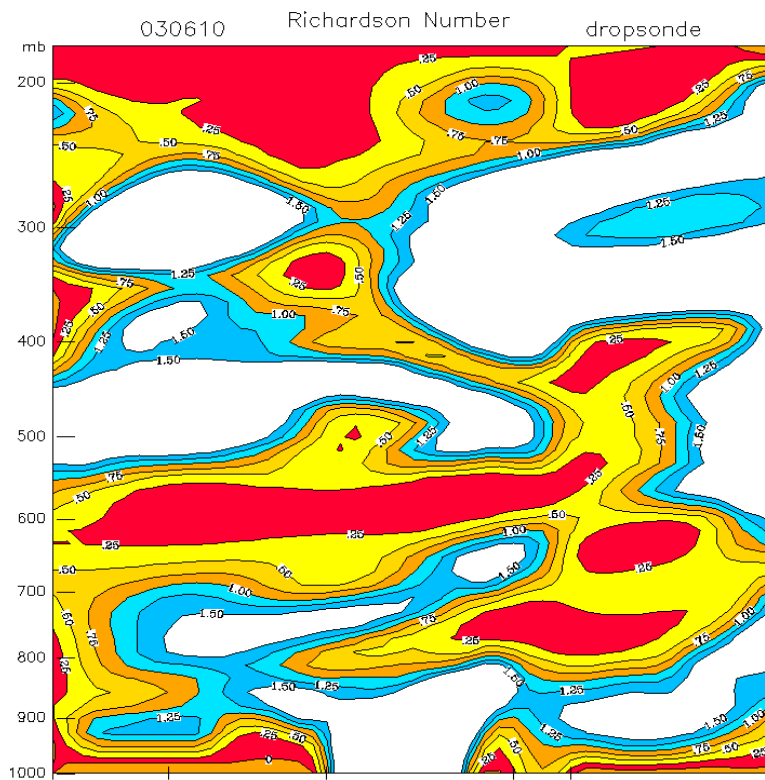
Fig. 8. Same as Fig. 7 except for Richardson's number.
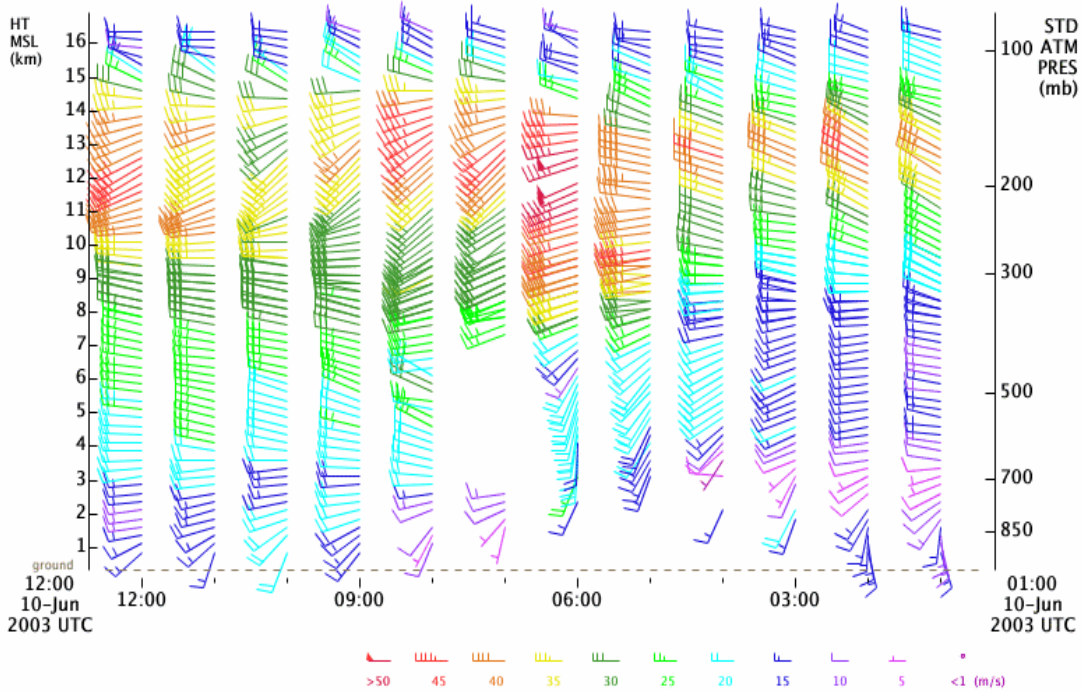
Fig. 9. Wind profiler observations at Slater, Iowa, wind profiler site. See
Fig. 3 for location. Profiler data is avilable at the website
http://www.profiler.noaa.gov/jsp/profiler.jsp
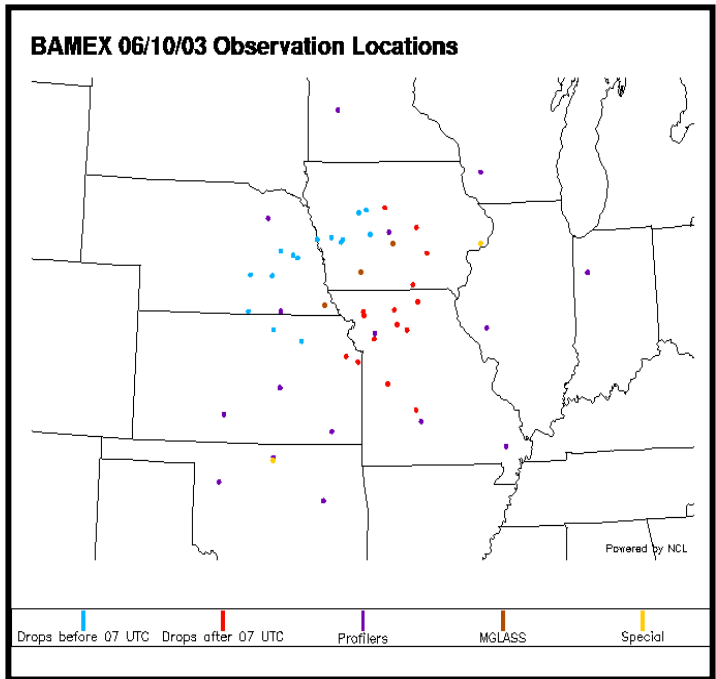
Fig. 10. Geographic location of soundings used in construction of quadrant composite wind profiles. Colors indicate observation type and period of dropsonde launches.
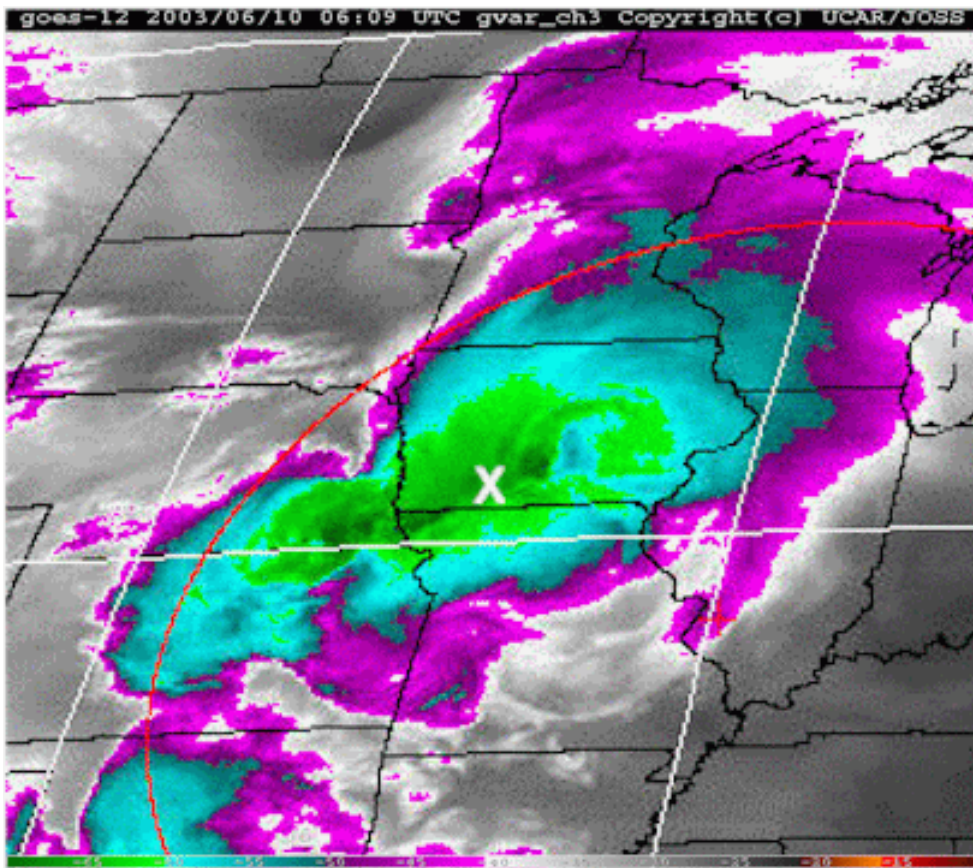
Fig. 11. Water vapor imagery at 0609 UTC. The white "x" indicates anvil center anchor point used to construct composite fields.
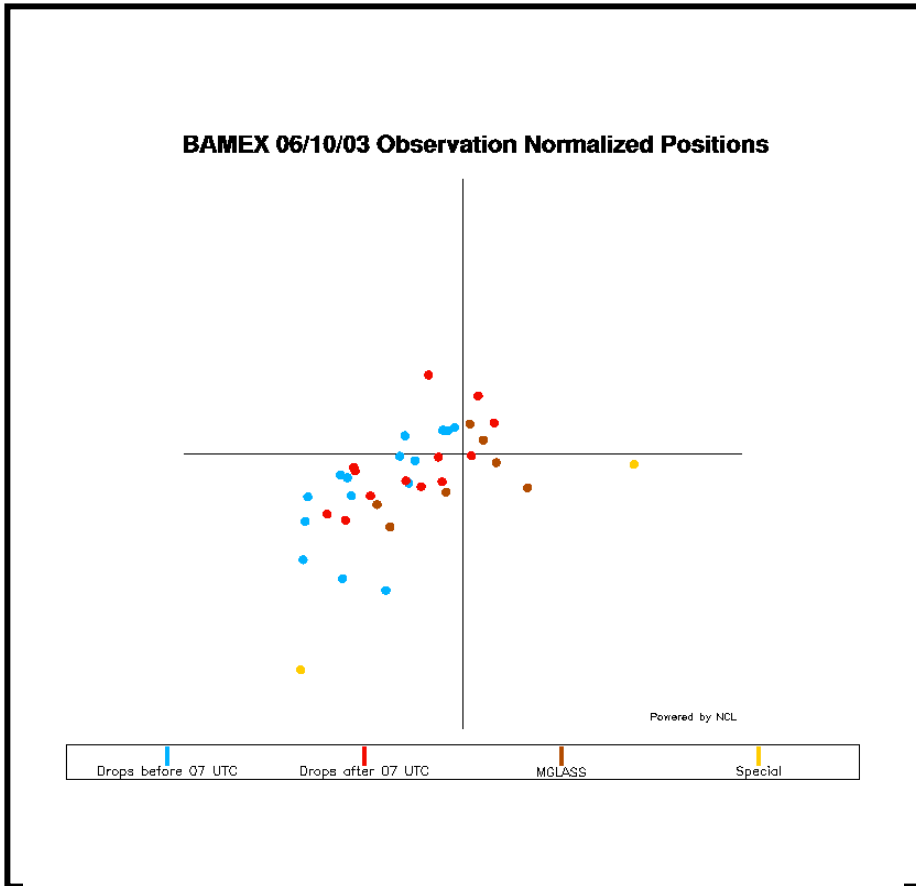
Fig.12. MCS anvil-relative observation sites for composite construction.
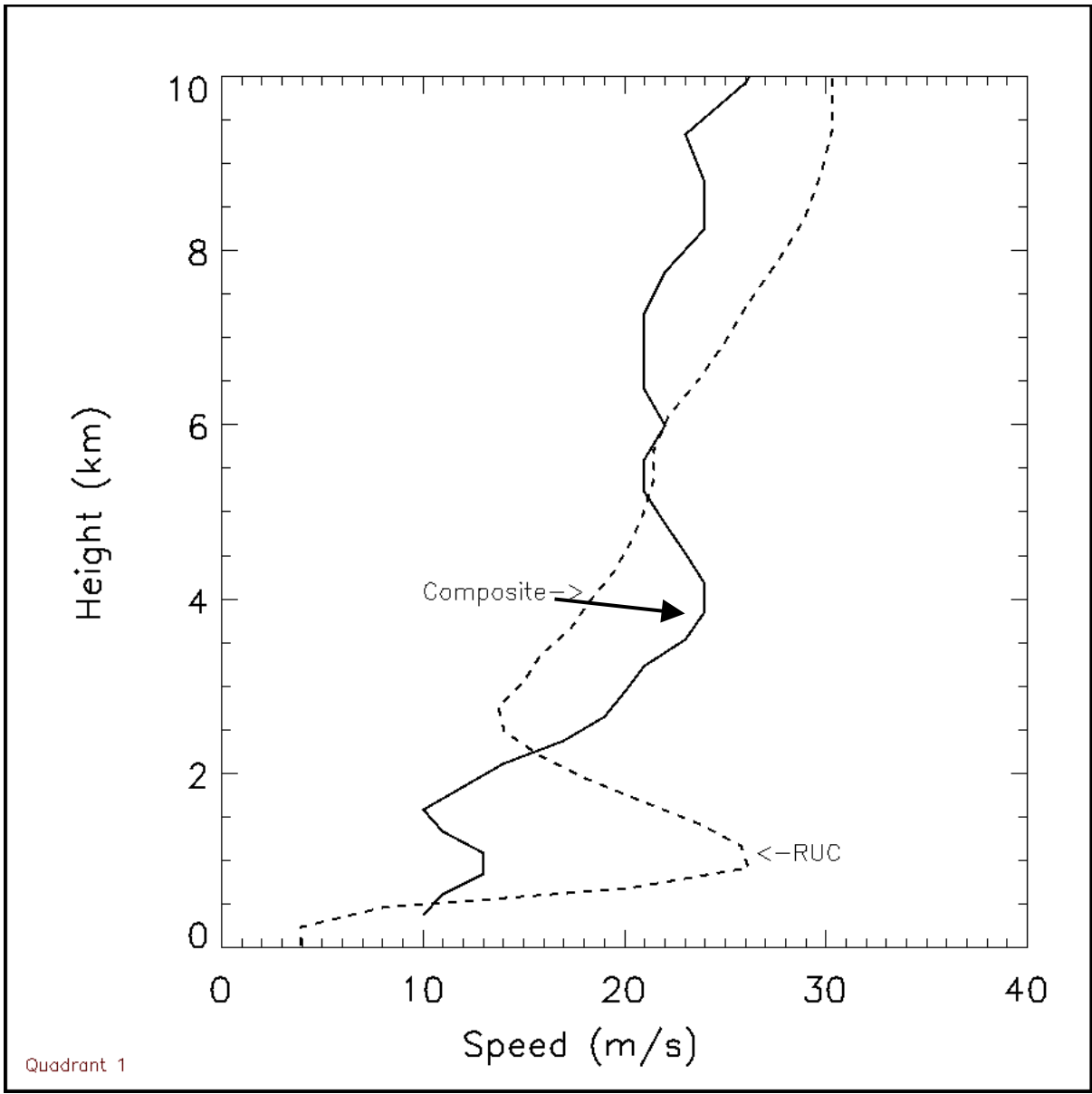
Fig. 13. Windspeed profiles in the Northwest (NW) quadrant (cf. Fig. 12) as computed from composited dropsonde wind profiles (solid curve) and as analyzed by the RUC model assimilation system at 0700 UTC.
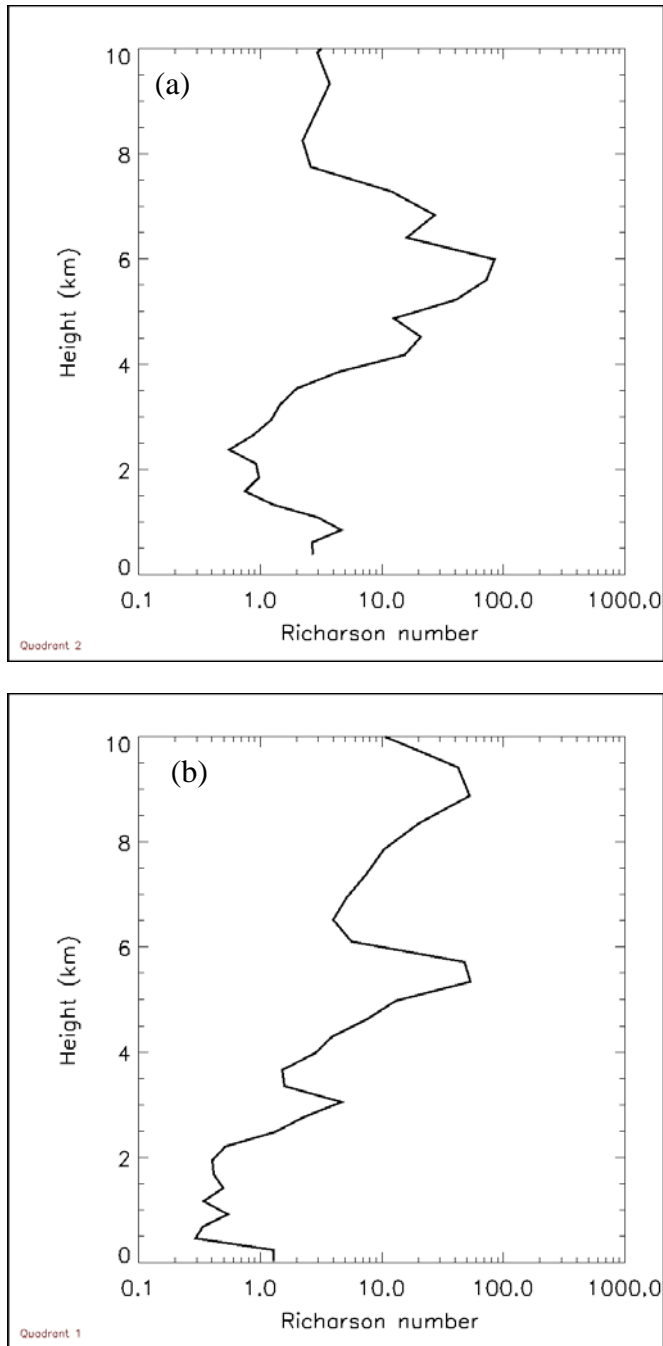
Fig. 14. Same as Fig. 13 except for Richardson's Number (Ri) computed using (a) composite data and (b) 0700 UTC RUC analysis fields.
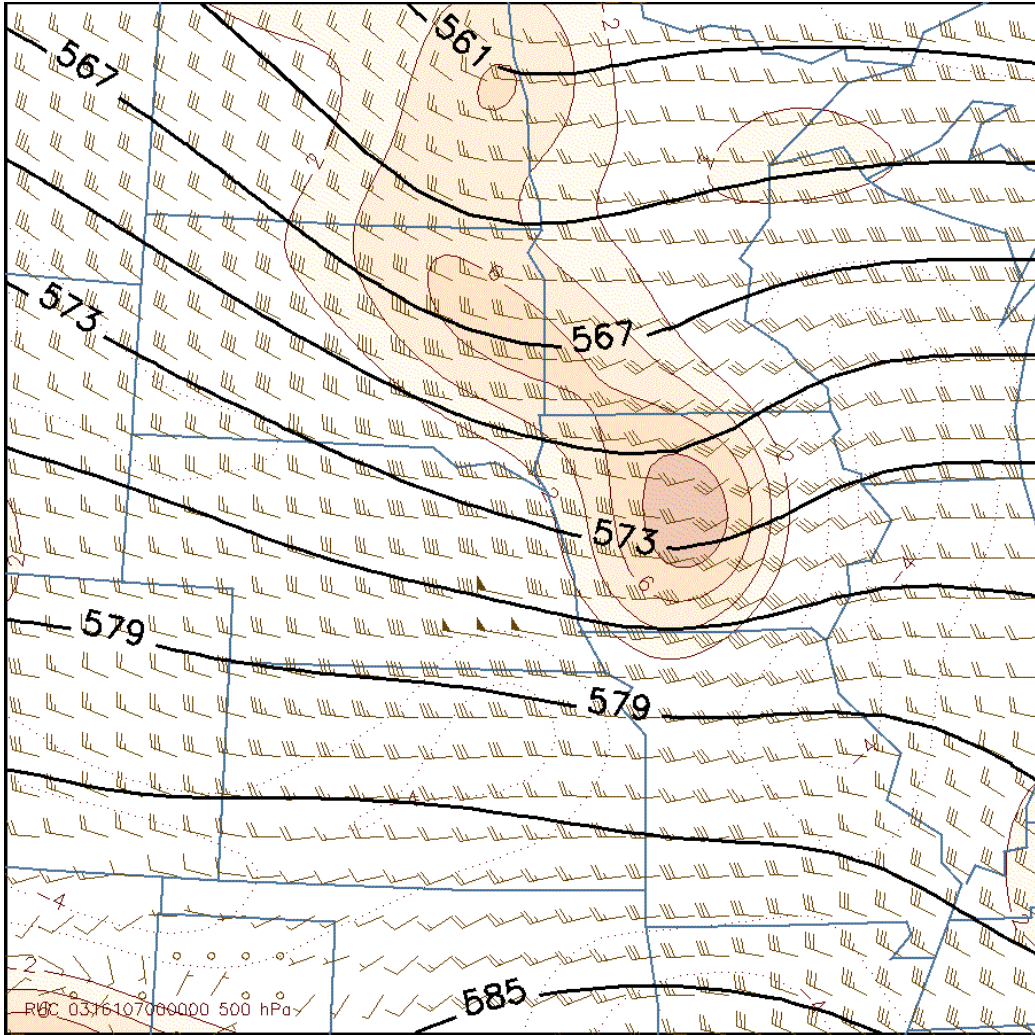
Fig. 15. RUC analysis fields at 0700 UTC 10 June at 500 mb. Colored shading indicates regions of positive vorticity, heavy contour lines are geopotential height in decameters, and winds are in kt.
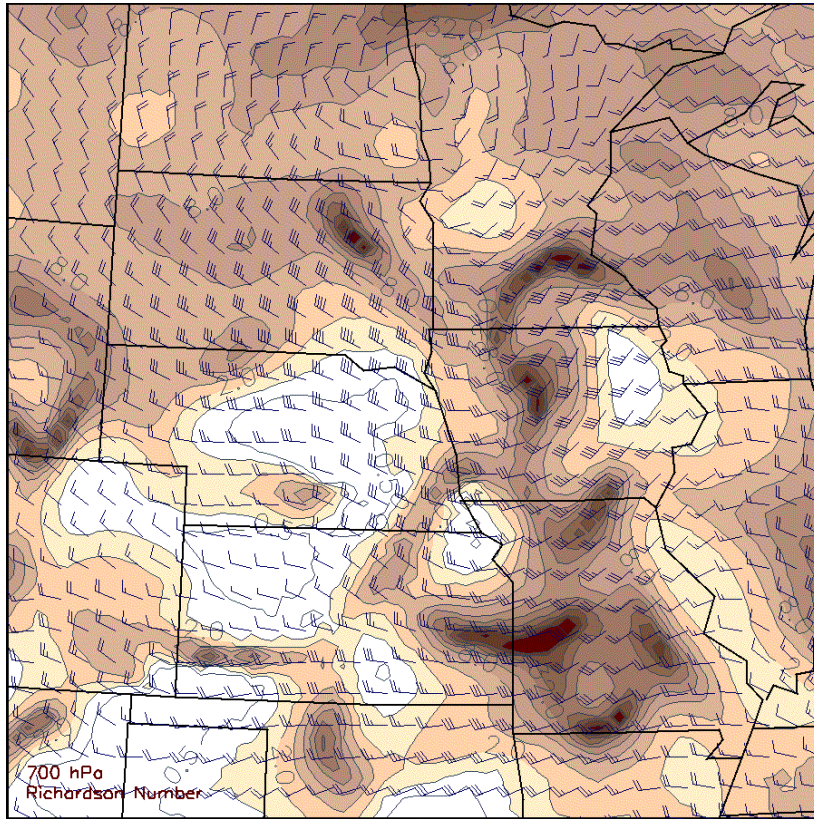
Fig. 16. RUC analysis of Richardson number at 0700 UTC 10 June at 700 mb (shading). Smaller (white) values approach turbulence thresholds. Wind barbs are in kt.
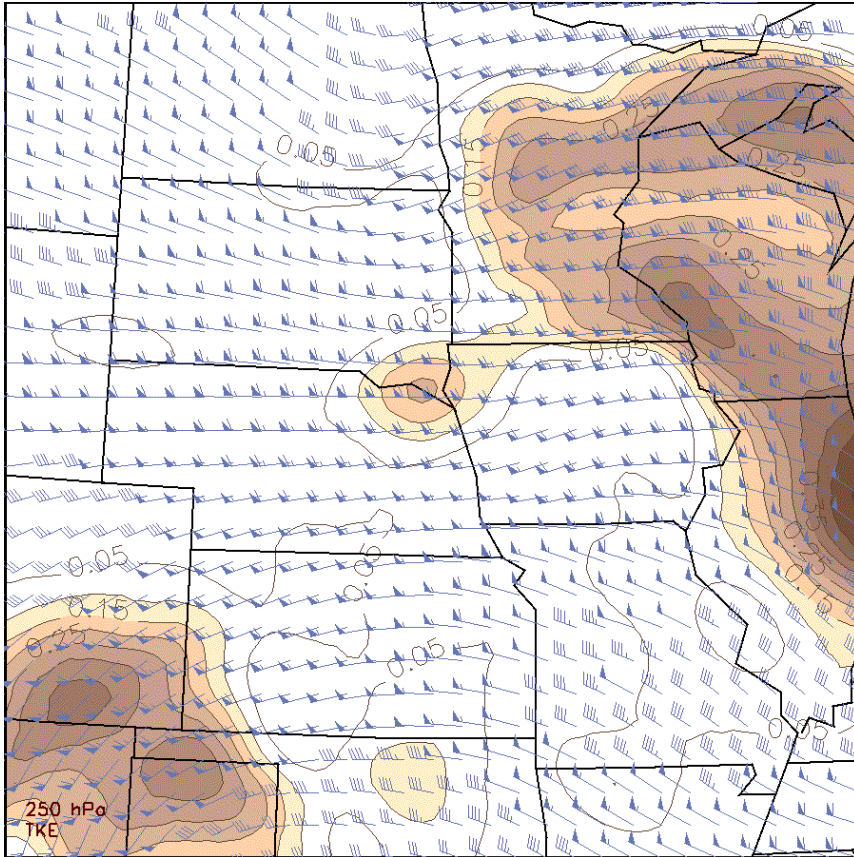
Fig. 17. RUC analysis of DTF3-computed turbulent kinetic energy (TKE) at 0700 UTC 10 June at 250 mb (shading). Wind barbs are in kt.
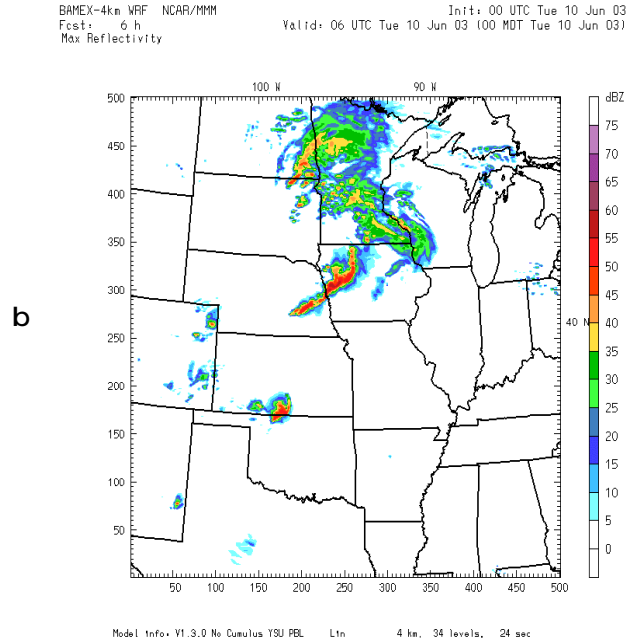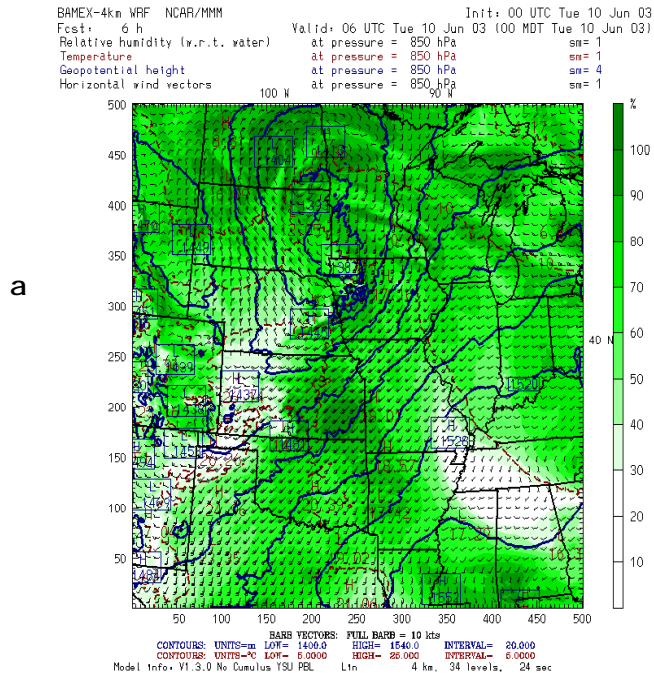
Fig. 18. 6h 4km WRF forecasts valid at 0600 10 June 2003 for (a) winds, relative humidity (green shading), temperature (red dashed contours), and geopotential (blue contours), and (b) reflectivity.
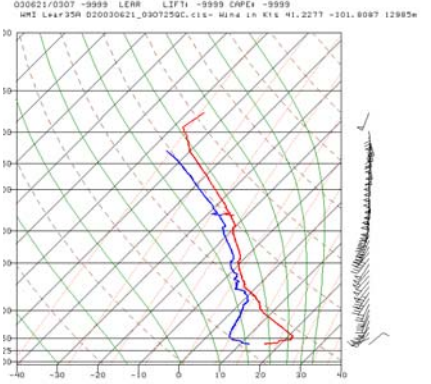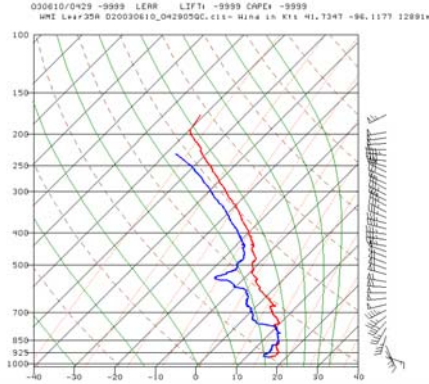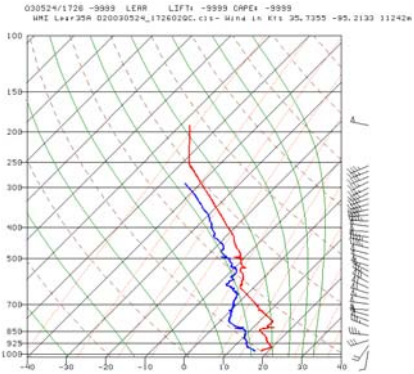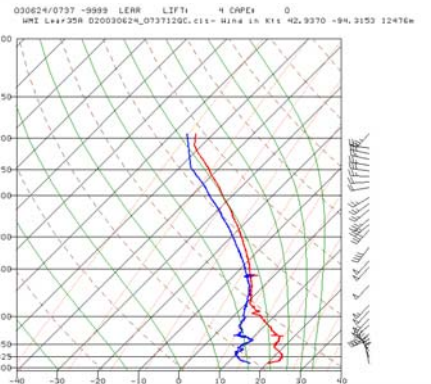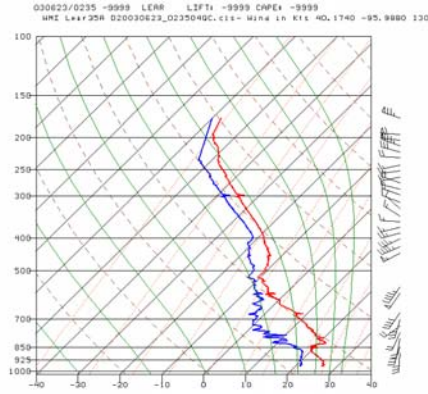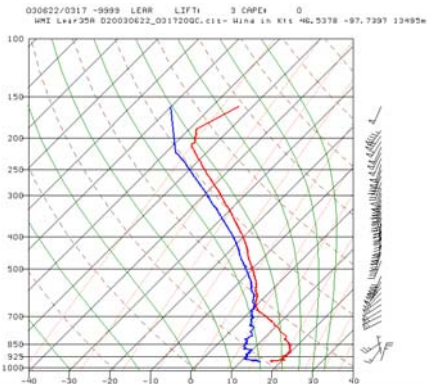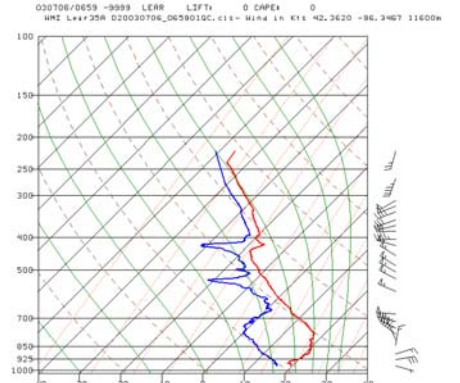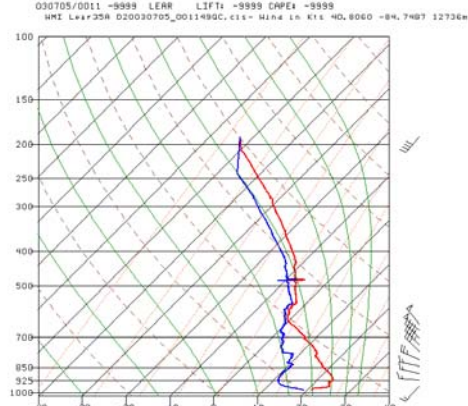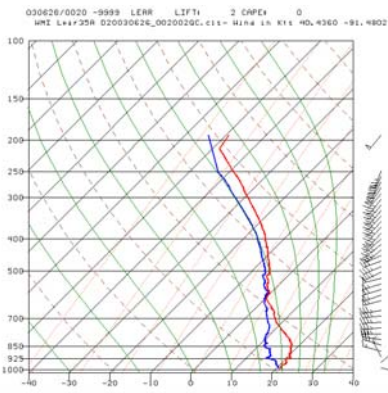
Fig. 19. Skew-t diagrams of rear inflow regions of BAMEX cases produced
from dropsondes launched on dates and times indicated.
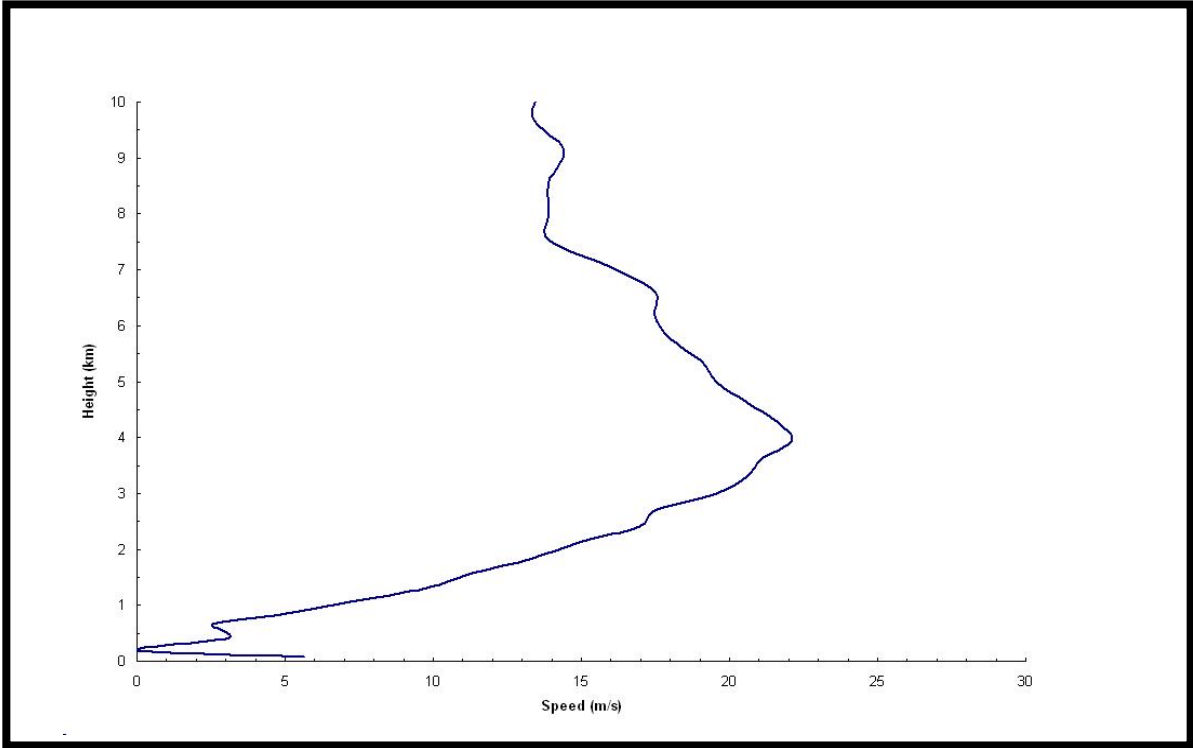
Fig. 20. Composite profile of MCS rear inflow produced from the nine cases presented in Fig. 19.